Eur. J. Mineral.
2017, **29**, 689–700
Published online 31 May 2017

Special issue dedicated to Zdeněk Johan

Écrinsite, $AgTl_3Pb_4As_{11}Sb_9S_{36}$, a new thallium-rich homeotype of baumhauerite from the Jas Roux sulphosalt deposit, Parc national des Écrins, Hautes-Alpes, France

DAN TOPA[1,*], UWE KOLITSCH[1,2], EMIL MAKOVICKY[3] and CHRIS STANLEY[4]

[1] Naturhistorisches Museum, Burgring 7, 1010 Wien, Austria
*Corresponding author, e-mail: dan.topa@nhm-wien.ac.at
[2] Institut für Mineralogie und Kristallographie, Universität Wien, Althanstraße 14, 1090 Wien, Austria
[3] Department of Geoscience and Resource Management, University of Copenhagen, Østervoldgade 10, 1350 Copenhagen K, Denmark
[4] Natural History Museum, Cromwell Road, London SW7 5BD, UK

Abstract: Écrinsite, ideally $AgTl_3Pb_4As_{11}Sb_9S_{36}$, is a new thallium sulphosalt species found in the Jas Roux As–Sb–Pb–Tl–Hg–Ag deposit, Parc national des Écrins, Département des Hautes-Alpes, France. Associated minerals in four different samples are jasrouxite, stibnite, smithite, guettardite, chabournéite, pierrotite and As-bearing zinkenite. Écrinsite is opaque with metallic lustre. It is brittle without any discernible cleavage and with conchoidal fracture. In reflected light écrinsite is white, pleochroism is not discernible. Internal reflections are absent. In crossed polarisers, anisotropism is distinct, with rotation tints in shades of grey. The reflectance data (%, air) are: 37.3, 38.6 at 470 nm, 35.2, 36.7 at 546 nm, 34.0, 35.5 at 589 nm and 32.0, 33.3 at 650 nm. Mohs hardness is 3–3½, microhardness VHN_{25} is in the range 175–201, with a mean value of 189 kg mm^{-2}. Average results of 20 electron-microprobe analyses for the structurally investigated grain are (in wt%): Ag 2.03(10), Cu 0.02(1), Tl 14.57(20), Pb 16.23(32), Sb 23.97(25), As 17.87(17), S 25.20(15), total 99.88 (15), corresponding to $Ag_{0.87}Cu_{0.02}Tl_{3.28}Pb_{3.61}Sb_{9.06}As_{10.98}S_{36.19}$ (on the basis of $28Me + 36S = 64$ *apfu*). The simplified formula, $AgTl_3Pb_4Sb_9As_{11}S_{36}$, is in accordance with the results of the crystal-structure analysis and may be derived from the ideal baumhauerite formula, $Pb_{12}As_{16}S_{36}$, by substitution of Sb for As and $[(Tl,Ag)^{+} + (As,Sb)^{3+}] \leftrightarrow 2Pb^{2+}$. The density, 4.96 g cm^{-3}, was calculated using the ideal formula. Écrinsite has a triclinic cell, space group $P\bar{1}$, with $a = 8.080(2)$, $b = 8.533(2)$, $c = 22.613(4)$ Å, $\alpha = 90.23(3)°$, $\beta = 97.17(3)°$, $\gamma = 90.83(3)°$, $V = 1546.7(6)$ Å^3, and $Z = 1$. The strongest five lines in the (calculated) powder-diffraction pattern are [*d* in Å(*I*)(*h k l*)]: 4.14(68)(1 0 5), 3.72(92)(1 0 5), 3.56(100)(1 0 6), 3.53(80)(1 2 2) and 3.48(72)(1 2 2). Écrinsite is a new member of the sartorite homologous series with $N_{1,2} = 3$, 4, *i.e.*, $N = 3.5$. Four other members share the same N value as écrinsite: baumhauerite, argentobaumhauerite, boscardinite and bernarlottiite. By comparison to the closely related boscardinite (ideally $Tl_2Pb_8Sb_{14}As_4S_{36}$), écrinsite is characterised by both an excess of As over Sb and a distinctly higher substitution of $[(Tl,Ag)^{+} + (As,Sb)^{3+}] \leftrightarrow 2Pb^{2+}$. Baumhauerite and bernarlottiite are basically unsubstituted members, whereas argentobaumhauerite has a Ag substitution, without Tl.

Key-words: écrinsite; sulphosalt; new mineral; thallium; crystal structure; sartorite homologous series; Jas Roux deposit; Parc national des Écrins; France.

1. Introduction

In the last decades, the sartorite homologous series, known originally from the classical sulphosalt localities of Lengenbach, Binn Valley (Wallis, Switzerland), and Madoc (Ontario, Canada), has been enriched by additional members, both with new chemical compositions and from new localities. Among the latter are Moosegg mine, Salzburg, Austria (Graeser *et al.*, 1986; Topa & Makovicky, 2016), Barika ore deposit, Iran (Makovicky *et al.*, 2012; Topa *et al.*, 2013b), Monte Arsiccio mine, Tuscany, Italy (Orlandi *et al.*, 2012) and Pollone mine, Tuscany, Italy (Biagioni *et al.*, 2014; Topa *et al.*, 2017). The famous As–Sb–Pb–Tl–Hg–Ag Jas Roux deposit in the Parc national des Écrins, Département des Hautes-Alpes, France (Johan & Mantienne, 2000; Bourgoin *et al.*, 2011), is also among these, having yielded six new mineral species.

Owing especially to improved analytical facilities and new research material, the originally pure Pb–As $N = 3$, $4 = 3.5$ member of the sartorite homologous series (Makovicky, 1985), baumhauerite (ideally $Pb_{12}As_{16}S_{36}$) is now "accompanied" on its homologue composition line in the Pb–(As,Sb)–(Ag,Tl) diagram by argentobaumhauerite (Topa & Makovicky, 2016), boscardinite (Orlandi *et al.*, 2012; Biagioni & Moëlo, 2017), bernarlottiite (Orlandi *et al.*, 2017) and now by one additional sulphosalt, écrinsite, described in this contribution. All four minerals have in common the 1:1 alternation of a three-polyhedra double-

DOI: 10.1127/ejm/2017/0029-2639
0935-1221/17/0029-2639 $ 5.40

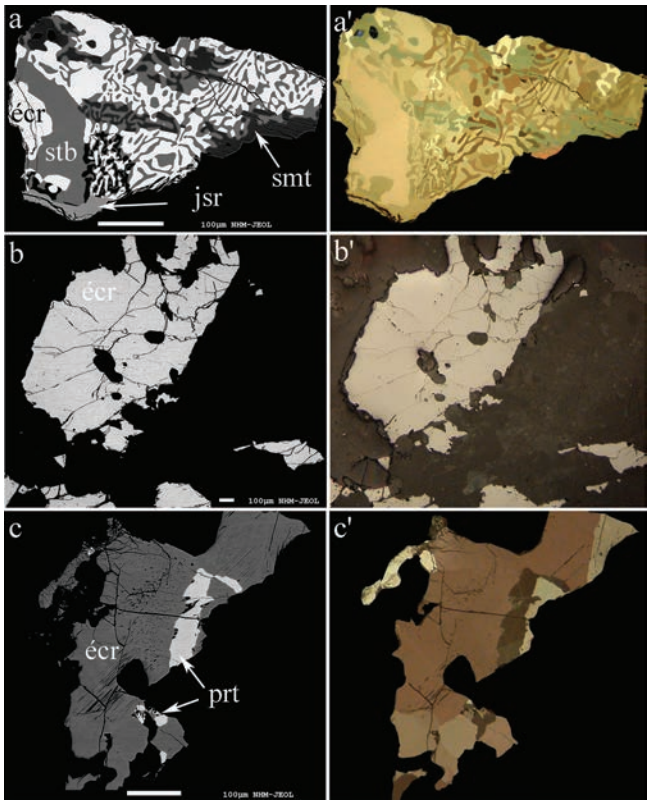

Fig. 1. Backscattered electron images and corresponding reflected-light photographs (crossed polarisers) of écrinsite and associated phases. (a, a′) A myrmekitic aggregate of écrinsite (écr), stibnite (stb) and smithite (smt) with jasrouxite (jsr) remnants, from sample JR (écrinsite no. 5 in Table 2). (b, b′) A large homogeneous écrinsite grain (no. 4 in Table 2) from sample J5R1. (c, c′) Écrinsite (écr) with pierrotite (prt) from sample HG (écrinsite no. 2 in Table 2).

chain ribbon ($N=3$) with a four-polyhedra double-chain ribbon ($N=4$). In argentobaumhauerite, small amounts of Ag substitute together with As for Pb, in bernarlottiite Sb-for-As substitution modifies the structure. The latter is joined by Tl and (As,Sb) substitution for Pb in boscardinite, whereas in écrinsite the latter substitutions are joined by an Ag substitution, resulting in the most complex combination of cation substitutions within this series. The presence of Tl- and Ag-substitutions differentiates écrinsite from bernarlottiite and the pure Pb–As members, and especially the completely different As/Sb ratio from type boscardinite.

While working on jasrouxite type material, a phase initially labelled "boscardinite-like material" was found in association with jasrouxite (Topa *et al.*, 2013a) and, although from chemical analyses the ratio Sb/As indicated a clear departure from type boscardinite itself, no single-crystal study was conducted at that time. New samples and a careful investigation of old samples now made possible a full characterization of this phase and its description as a new mineral species, écrinsite.

The name of the new mineral is for the Parc national des Écrins, Département des Hautes-Alpes, France, in which the type locality (Jas Roux) is located. The mineral and the mineral name were approved by the IMA-CNMNC (IMA 2015-099). The holotype is deposited in the reference collection of the Naturhistorisches Museum, Wien, Austria, with catalogue number N 9870.

Table 1. Reflectance values (%) for écrinsite in air (WTiC standard).

λ (nm)	R_{min}	R_{max}	λ (nm)	R_{min}	R_{max}
400	38.6	39.3	560	34.9	36.4
420	38.3	39.1	580	34.3	35.8
440	38.0	38.9	**589**	**34.0**	**35.5**
460	37.6	38.7	600	33.7	35.1
470	**37.3**	**38.6**	620	32.9	34.4
480	37.0	38.4	640	32.3	33.7
500	36.5	38.0	**650**	**32.0**	**33.3**
520	36.0	37.5	660	31.6	33.0
540	35.4	36.9	680	31.2	32.5
546	**35.2**	**36.7**	700	30.8	32.2

The reference wavelengths required by the Commission on Ore Mineralogy (COM) are given in bold.

2. Occurrence

The Jas Roux As–Sb–Pb–Tl–Hg–Ag deposit is situated in a Triassic metasedimentary series overlying the junction of three major lithostratigraphic basement units forming the Pelvoux Massif in the Département des Hautes-Alpes, France (Mantienne, 1974; Johan & Mantienne, 2000). Both synsedimentary and hydrothermal pyrite are present in the sediment-hosted deposit; sphalerite is characterised by low Cd, Fe and Tl contents (Johan & Mantienne, 2000). Bourgoin *et al.* (2011) give a list of the primary ore mineral species of the deposit as follows (in alphabetical order; ∗ signifying that Jas Roux is type locality): aktashite (Zn-bearing), "andorite" (As-bearing), chabournéite∗, getchellite, laffittite∗, parapierrotite, pierrotite∗, pyrite, realgar (abundant), routhierite∗, smithite, sphalerite, stibnite, twinnite, wakabayashilite and zinkenite (As-bearing). Johan & Mantienne (2000) also describe four unnamed species: $(Pb,Tl)_9Ag(Sb,As)_{13}S_{29}$ (related to either jamesonite or madocite), $Tl(As,Sb)_{10}S_{16}$ (X-ray amorphous), $Tl(Sb,As)_7S_{11}$ and $Ag_2(Sb,As)S_4$ (reaction product between smithite and chabournéite). Recently, the new mineral jasrouxite, $Ag_{16}Pb_4Sb_{24}As_{16}S_{72}$, was described by Topa *et al.* (2013a); it was collected in 2011 during a study of the Jas Roux deposit which was authorized by the administration of the Parc national des Écrins. A small number of secondary minerals comprise klebelsbergite, scorodite, valentinite and several sulphates (Bourgoin *et al.*, 2011).

The mineralization sequence comprises four stages (Johan & Mantienne, 2000; Bourgoin *et al.*, 2011). Stage I: pyrite–sphalerite–lead sulphosalts–stibnite. Stage II is characterized by a predominance of As–Sb and Tl, at the beginning also with Pb, producing chabournéite. The late Tl–As–Hg–Ag minerals of stage III, with a subdued role of Cu, are disseminated throughout the central block and replace the previously formed phases. Realgar (stage IV) concludes the mineralization process. The entire process is believed to have been caused by low-temperature

Table 2. Chemical composition of écrinsite (wt%) and empirical formulae calculated on the basis of 64 *apfu*.

No.	1	2	3	4	5	6
Grain group, Fig.	Group 1[c]	Group 2, Fig. 1c	Group 3	Group 4[c], Fig. 1b	In myrmekite[c]	Group 5
n[a]	20	8	21	33	10	23
Ag	2.03(10)	2.02(05)	2.11(09)	2.14(09)	1.98(09)	2.06(10)
Cu	0.02(01)	0.02(01)	0.02(01)	0.02(01)	0.05(01)	0.05(01)
Tl	14.57(20)	13.88(30)	12.80(30)	11.44(29)	8.63(21)	7.52(25)
Pb	16.23(32)	17.07(48)	19.22(48)	21.66(45)	26.72(28)	27.02(55)
Sb	23.97(25)	23.85(20)	23.82(19)	23.04(21)	21.27(20)	22.01(22)
As	17.87(17)	18.16(11)	17.02(15)	16.78(25)	16.67(22)	16.49(25)
S	25.20(15)	25.28(13)	24.86(19)	24.73(12)	24.39(08)	24.56(18)
Total	99.88(15)	100.28(1)	99.87(13)	99.84(11)	99.71(17)	99.75(39)
ch[b]	−1.4	−0.7	−1.0	−1.2	−0.7	−0.9
N_{chem}	3.50	3.45	3.52	3.52	3.49	3.40
Ag_{subst}	43.6	47.3	44.7	44.8	44.9	56.1
Tl_{subst}	54.8	53.6	48.3	43.2	33.7	30.9

No. 1: $Ag_{0.87}Cu_{0.01}Tl_{3.28}Pb_{3.61}(Sb_{9.06}As_{10.98})_{\Sigma 20.04}S_{36.19}$
No. 2: $Ag_{0.86}Cu_{0.01}Tl_{3.11}Pb_{3.78}(Sb_{8.98}As_{11.11})_{\Sigma 20.09}S_{36.14}$
No. 3: $Ag_{0.91}Cu_{0.01}Tl_{2.92}Pb_{4.32}(Sb_{9.11}As_{10.59})_{\Sigma 19.71}S_{36.13}$
No. 4: $Ag_{0.93}Cu_{0.02}Tl_{2.62}Pb_{4.90}(Sb_{8.87}As_{10.50})_{\Sigma 19.37}S_{36.15}$
No. 5: $Ag_{0.87}Cu_{0.04}Tl_{2.00}Pb_{6.12}(Sb_{8.29}As_{10.56})_{\Sigma 18.85}S_{36.11}$
No. 6: $Ag_{0.90}Cu_{0.03}Tl_{1.74}Pb_{6.17}(Sb_{8.54}As_{10.40})_{\Sigma 18.94}S_{36.21}$

[a] n – number of analyses.
[b] ch – charge balance ($\Sigma_{cation\ charges} - \Sigma_{anion\ charges}$) based on at%. N_{chem}, Ag_{subst} and Tl_{subst} are defined in Makovicky (1985) and Makovicky & Topa (2015).

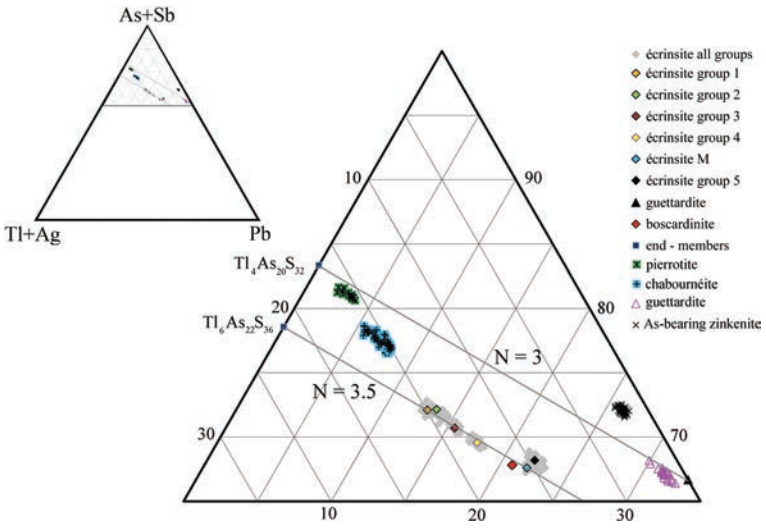

Fig. 2. Substitution variations in écrinsite and associated ore minerals from Jas Roux in the Pb–(As+Sb)–(Tl+Ag) sulphide system (at%) with the relevant substitution lines indicated. The composition of type boscardinite is also indicated for comparison. For analytical data of the associated phases see Table 3.

hydrothermal fluids of Triassic age, similar to the present-day active geothermal systems (Johan & Mantienne, 2000). However, the role of an Alpine, Tertiary remobilization may have been important, especially along faults that cut the mineralization into several blocks (Mantienne, 1974). Organic-matter reflectance and fluid-inclusion studies in the Paleocene prehnite–pumpellyite-facies metagreywackes transgressive on the southern Pelvoux massif suggest that temperature there did not exceed the 200–300 °C range during Alpine times (Stalder, 1979; Saliot *et al.*, 1982).

3. Appearance and physical properties

Two specimens (J5R1 and J6R5) containing the phase that later turned out to be écrinsite were received from G. Favreau and V. Bourgoin in 2014, beside the deposited type-locality sample of jasrouxite (JR, Fig. 1a and a′); these samples were collected *in situ* [with administrative permission] in the area "C2" of Bourgoin *et al.* (2011). Additionally, H. Geuer supplied the first author with another écrinsite-bearing sample (HG, Fig. 1c and c′) of Jas Roux material; it is unknown when and from which area this sample was originally collected.

Écrinsite forms anhedral crystal aggregates attaining a size of up to 400 μm and only one crystal aggregate ranging up to more than 1.5 mm across (deposited holotype sample J5R1, Fig. 1b and b′). The mineral also rarely forms prismatic crystals with complex forms (not measurable), without visual indications of twinning. Écrinsite is opaque, its colour is dark grey, and it has black streak and metallic lustre. Mohs hardness has been estimated as 3–3½, based on the microhardness values (VHN_{25} range 175–201, mean 189 kg mm^{-2}). Écrinsite is brittle, without cleavage and

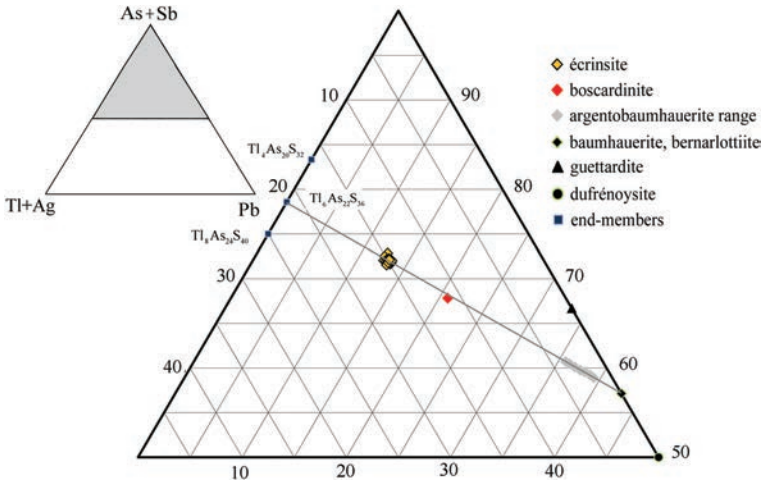

Fig. 3. Position of structurally analysed écrinsite in the Pb–(As+Sb)–(Tl+Ag) sulphide system (at%) with the relevant sartorite homologues added.

Table 3. Composition of minerals associated with écrinsite (wt%) and empirical formulae calculated on the basis of 5, 4, 60, 56, 60 and 73 *apfu* for stibnite, pierrotite, chabournéite, guettardite and zinkenite, respectively (Moëlo *et al.*, 2008).

No.	1 As-bearing stibnite	2 Sb-bearing smithite	3 Pierrotite	4 Chabournéite	5 Guettardite	6 As-bearing zinkenite
n[a]	6	3	6	8	22	6
Ag	0.00	42.15(10)	0.07(05)	0.12(05)	0.00	0.88(12)
Cu	0.09(02)	0.00	0.02(01)	0.00	0.00	0.16(02)
Tl	0.00	0.17(01)	19.42(05)	18.45(16)	1.49(30)	0.00
Pb	0.00	0.00	4.36(27)	10.00(18)	37.24(61)	31.40(46)
Sb	66.40(15)	8.36(12)	33.47(08)	27.93(24)	21.56(40)	30.06(23)
As	4.54(08)	24.22(04)	16.57(24)	17.91(19)	15.48(42)	12.63(19)
S	28.95(14)	25.34(06)	26.16(10)	25.83(13)	24.31(23)	24.96(13)
Total	99.98(20)	100.24(1)	100.07(3)	100.24(1)	100.08(3)	100.09(1)
ch[b]	0.8	−0.9	−0.4	−1.2	0.1	0.1
N_{chem}			3.06	3.23	3.03	
Tl_{subst}			87.7	78.2		

No. 1: $Sb_{1.81}As_{0.20}S_{2.99}$, No. 2: $Ag_{0.99}Sb_{0.17}As_{0.82}S_{2.01}$, No. 3: $Ag_{0.03}Cu_{0.01}Tl_{3.72}Pb_{0.83}Sb_{10.77}As_{8.67}S_{31.97}$, No. 4: $Ag_{0.05}Tl_{3.83}Pb_{2.05}Sb_{9.74}As_{10.15}S_{34.19}$, No. 5: $Tl_{0.31}Pb_{7.58}Sb_{7.46}As_{8.71}S_{31.95}$ and No. 6: $Ag_{0.44}Cu_{0.13}Pb_{8.16}Sb_{13.29}As_{9.08}S_{41.91}$.

[a] n – number of analyses.

[b] ch – charge balance ($\Sigma_{cation\ charges} - \Sigma_{anion\ charges}$) based on at%. N_{chem} and Tl_{subst} are defined in Makovicky (1985) and Makovicky & Topa (2015).

with conchoidal fracture. The density could not be measured because of paucity of available material. It was calculated as 4.96 g cm^{-3} using the ideal chemical formula and the measured single-crystal unit-cell parameters. The a:b:c ratio calculated from the unit-cell parameters is 0.9496:1:2.6501.

In reflected light, the colour of écrinsite is white, with weak bireflectance in air (Table 1), no discernible pleochroism and distinct anisotropy. Rotation tints vary between different shades of grey. No internal reflections were seen.

4. Chemical data

Chemical analyses of écrinsite and associated minerals were carried out using a JEOL JXA 8530F field-emission gun electron microprobe (EMP) in the Zentrale Forschungslaboratorien at the Naturhistorisches Museum, Wien, employing JEOL and Probe for EMP analysis software (WDS mode, 25 kV, 20 nA, 2 μm beam diameter, count time 10 s on peak and 5 s on background positions). The following emission lines and standards were used: As-$L\alpha$, Tl-$L\alpha$ and S-$K\alpha$ (lorándite, $TlAsS_2$), Pb-$M\alpha$ (galena), Ag-$L\alpha$ (Ag metal), Cu-$K\alpha$ (chalcopyrite) and Sb-$L\alpha$ (stibnite). Other elements (Hg, Bi and Fe) were sought but not detected. Before the standard correction of the raw X-ray intensities for matrix effects with the JEOL-ZAF procedure, an empirical correction for As-$L\alpha$ peak overlap with the third-order Sb-$L\alpha$ peak was applied.

The mean chemical compositions of écrinsite crystals with different degree of substitution are presented in Table 2 and plotted in the (As+Sb)–Tl–Pb ternary diagram (Fig. 2). The chemical composition of the grains used for structural studies is marked. The low amounts of Cu are above the detection limit (~100 ppm) of Cu in an écrinsite matrix.

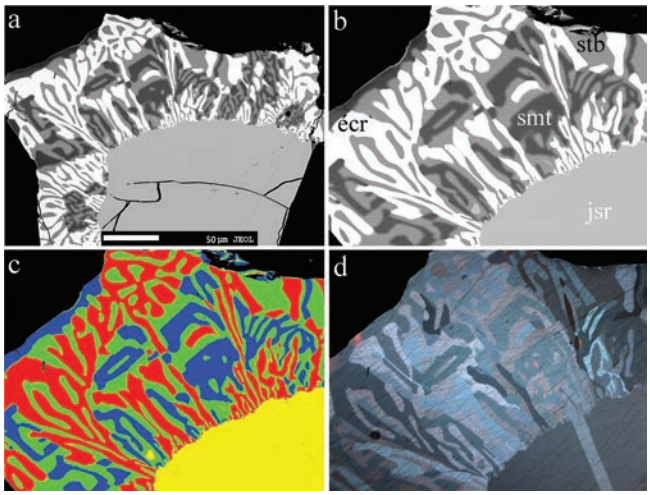

Fig. 4. Homogeneous grains of jasrouxite (jsr) in JR sample, covered and replaced by a composite three-phase myrmekitic aggregate composed of stibnite (stb), écrinsite (écr) and smithite (smt) in intimate intergrowth. (a, b) Backscattered images, (c) false-colour image of (b) (blue, smithite; green, stibnite; red, écrinsite) and (d) reflected-light photographs (crossed polarisers, note the domain-like texture).

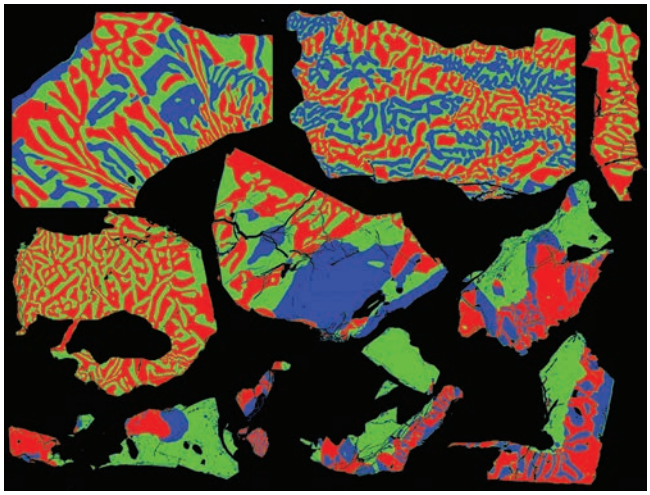

Fig. 5. Backscattered electron composite images of the three-phase myrmekite aggregates, illustrated in false colours (blue, smithite; green, stibnite; red, écrinsite).

Table 4. Crystal data and summary of parameters describing data collection and refinement for holotype écrinsite.

Crystal data	
Chemical formula	$Ag_{0.87}Tl_{3.28}Pb_{3.61}As_{10.98}Sb_{9.06}S_{36.19}$
Formula weight (g)	13437.8
Crystal system	Triclinic
Space group	*P*1 (no. 2)
a (Å)	8.0802(1)
b (Å)	8.5332(2)
c (Å)	22.6122(4)
α (°)	90.233(1)
β (°)	97.174(1)
γ (°)	90.832(1)
V (Å^3)	1546.71(5)
Z	1
D_x (Mg m^{-3})	4.96
μ (mm^{-1})	29.86
Crystal form	Irregular
Crystal size (mm)	0.015 × 0.04 × 0.07
Data collection	
T_{min}, T_{max}	0.34, 0.75
Measured reflections	21 978
Independent reflections	11 124
Observed reflections	6199 [$I > 2\sigma(I)$]
R_{int} (%), $R_{(sigma)}$ (%)	11.66, 8.87
θ_{max} (°)	32.65
Range of *h*, *k*, *l*	$-12 \le h \le 12$, $-12 \le k \le 12$, $-34 \le l \le 34$
Structure refinement	
Refinement on F_o^2	
$R[F_o > 4\sigma(F_o)]$ (%)	5.25
$wR(F_o^2)$ (%)	12.31
S (GoF)	1.051
Reflections in refinement	11 124
Parameters refined	311
Weighting scheme[a]	$a = 0.051$, $b = 0.142$
$(\Delta/\sigma)_{max}$	0.002
$\Delta\rho_{max}$ (e Å^{-3})	3.15 (0.07 Å from As10)
$\Delta\rho_{min}$ (e Å^{-3})	−3.73 (0.76 Å from Pb4)
Extinction coefficient	None
Source of atomic scattering factors	*International Tables for X-Ray Crystallography* (1992, Vol. C, Tables 4.2.6.8 and 6.1.1.4)

[a] $w = 1/[\sigma^2(F_o^2) + (aP)^2 + bP]$, where $P = (F_o^2 + 2F_c^2)/3$.

The empirical formulae (based on 64 atoms per formula unit (*apfu*), 28Me + 36S, from the results of the single-crystal study) are presented in a footnote of Table 2 for all analysed grain groups. The empirical formula is $Ag_{0.87}Cu_{0.01}Tl_{3.28}Pb_{3.61}(Sb_{9.06}As_{10.98})_{\Sigma 20.04}S_{36.19}$ for the grain with the highest Tl content. The simplified formula $AgTl_3Pb_4As_{11}Sb_9S_{36}$ is derived from the ideal baumhauerite formula, $Pb_{12}As_{16}S_{36}$, by the substitutions $Sb \leftrightarrow As$ and $[(Tl,Ag)^{+} + (As,Sb)^{3+}] \leftrightarrow 2Pb^{2+}$.

For all écrinsite-group analyses, the calculated N_{chem} values in Table 2 (Makovicky & Topa, 2015) cluster tightly around the theoretical and structurally determined value of $N = 3.5$ (Figs. 2 and 3). The percentage of the theoretical maximally Ag + (As,Sb)-substituted end-member, Ag_{subst} (procedure by Makovicky & Topa, 2015) varies between 43.6 and 56.1 mol%, whereas that of the theoretical fully substituted Tl + (As,Sb) end-member without Pb, Tl_{subst}, varies broadly, from 30.9 to 54.8 mol %. Between the latter, maximum Tl-substitution value (coupled with the minimum Ag-substitution value; Table 2), and the minimum Tl-substitution value, the substitutions are evenly spread (Table 2).

The combined substitution by Tl and Ag in the structurally characterized grain, calculated according to Makovicky (1985), is quite high, 69.7% of the theoretical

Table 5. Atom fractional coordinates, site occupancy factors (sof) and equivalent isotropic displacement parameters (Å^2) in écrinsite.

Site	Atom(s)	sof	*x*	*y*	*z*	U_{eq}
Tl1	Tl	1	0.13994(6)	0.63847(5)	0.17148(2)	0.0391(1)
Tl2	Tl	0.82(2)	0.8459(9)	0.8664(4)	0.8277(1)	0.0392(7)
Pb2	Pb	0.18(2)	0.798(2)	0.8488(9)	0.8330(5)	0.031(2)
Pb3	Pb	0.645(5)	0.6847(2)	0.6521(2)	0.26312(7)	0.0426(4)
Sb	Sb	0.355(5)	0.6846(9)	0.6228(7)	0.2493(3)	0.0426(4)
Pb4	Pb	1	0.68174(6)	0.13954(6)	0.26256(2)	0.0509(2)
Sb1	Sb	1	0.56261(8)	0.39157(8)	0.10362(3)	0.0289(2)
Sb2	Sb	1	0.82564(8)	0.11274(7)	0.01969(3)	0.0256(2)
(As,Sb)3	As,Sb	0.803(7), 0.197	0.4488(1)	0.1135(1)	0.87679(4)	0.0292(3)
As4	As	1	0.1988(1)	0.3651(1)	0.00594(4)	0.0208(1)
(As,Sb)5	As,Sb	0.847(7), 0.153	0.0826(1)	0.3967(1)	0.33254(4)	0.0307(3)
(As,Sb)6	As,Sb	0.663(8), 0.337	0.1108(1)	0.8413(1)	0.34587(4)	0.0345(3)
Sb7	Sb	0.770(9)	0.8504(3)	0.3329(3)	0.4622(1)	0.0316(4)
As7	As	0.230(9)	0.818(2)	0.3545(17)	0.4649(7)	0.0316(4)
(As,Sb)8	As,Sb	0.894(8), 0.106	0.7936(1)	0.9003(1)	0.44080(4)	0.0300(3)
(Sb,As)9	Sb,As	0.799(8), 0.201	0.4257(1)	0.16161(9)	0.41249(3)	0.0329(3)
As10	As	0.529(2)	0.4771(3)	0.6079(3)	0.4431(13)	0.0313(3)
Ag10	Ag	0.471(2)	0.4720(2)	0.6303(2)	0.41481(11)	0.0313(3)
S1	S		0.3656(3)	0.1758(3)	0.05089(11)	0.0279(5)
S2	S		0.9292(3)	0.6939(3)	0.39941(11)	0.0293(5)
S3	S		0.2629(3)	0.9112(3)	0.85592(10)	0.0229(5)
S4	S		0.9181(3)	0.3970(3)	0.24217(12)	0.0305(5)
S5	S		0.6264(3)	0.3591(3)	0.37815(10)	0.0262(5)
S6	S		0.6733(3)	0.1690(3)	0.51483(11)	0.0278(5)
S7	S		0.9928(3)	0.0960(3)	0.93398(09)	0.0220(5)
S8	S		0.9369(3)	0.8743(3)	0.25895(10)	0.0263(5)
S9	S		0.3416(3)	0.5719(3)	0.05501(10)	0.0238(5)
S10	S		0.3010(3)	0.4182(3)	0.47436(13)	0.0336(6)
S11	S		0.9682(3)	0.0919(3)	0.41495(14)	0.0384(7)
S12	S		0.9874(3)	0.3481(3)	0.06572(10)	0.0231(5)
S13	S		0.5754(3)	0.9195(3)	0.36568(12)	0.0350(6)
S14	S		0.2554(3)	0.2038(3)	0.30933(11)	0.0351(6)
S15	S		0.7244(3)	0.6773(3)	0.14449(10)	0.0247(5)
S16	S		0.2536(3)	0.6078(3)	0.31671(11)	0.0307(5)
S17	S		0.4556(3)	0.3825(3)	0.19901(10)	0.0262(5)
S18	S		0.5597(3)	0.1103(3)	0.78961(12)	0.0362(6)

Pb-free end-member. For the écrinsite grains of group 5 it drops even below the substitution percentage of type boscardinite (Orlandi *et al.*, 2012) (Figs. 2 and 3).

The empirical formulae of all analysed écrinsite crystals show a very constant Ag content (~0.9 *apfu*), slightly variable Tl contents (~1.5 *apfu*) coupled with similarly variable Pb ones (~3 *apfu*) coupled to a slightly decreasing Sb+As content (*apfu*).

5. Associated minerals and comparable phases

Homogeneous grains of jasrouxite in the JR samples are covered or embayed by composite three-phase myrmekitic aggregates composed of stibnite, écrinsite and smithite in intimate intergrowth (Figs. 1a, a′ and 4a–d). Remnants of jasrouxite in the "base" portions of the myrmekites are rare. The myrmekitic texture is finer at the base of the aggregate (*i.e.*, at the contact to the jasrouxite grains), turning into more isotropically lobed morphologies in the higher portions, away from the base. The myrmekites consist of large orientational domains; in each of them stibnite has a different orientation, as does écrinsite (Fig. 4d). Individual sinuous-shaped écrinsite grains are, however, rather full of lamellar twins on a fine scale. The general orientation of twinned aggregates changes when a stibnite "framework" changes its orientation. Smithite has the same anisotropy colours in all parts, independent of the orientation of accompanying phases. In some fragments, elongated myrmekitic blebs of stibnite and smithite alternate with, and are enveloped by, the interconnected elongated portions of myrmekitic aggregates which are composed of écrinsite and stibnite.

Polished sections prepared from sample J5R1 (Fig. 1b and b′) show only homogeneous écrinsite grains, those from sample HG show a constant association of écrinsite with pierrotite (Fig. 1c and c′), whereas those from sample J6R5 (not shown) reveal fine intergrowths of écrinsite with chabournéite, guettardite and As-bearing zinkenite (currently under study). Table 3 summarizes the mean chemical composition of the minerals associated with écrinsite in all investigated samples. The minerals were identified taking into account their position in the ternary plot (Fig. 2), empirical formulae and calculated N_{chem}, but single-crystal studies are needed to confirm these assumptions.

Table 6. Selected interatomic distances (Å) in écrinsite.

Tl1–		Tl2–		Pb2–		Pb3–		Sb–		Pb4–	
S18	3.250(3)	S14	3.157(3)	S17	2.852(13)	S15	2.750(3)	S15	2.477(7)	S3	2.803(2)
S4	3.263(3)	S18	3.175(4)	S18	3.056(9)	S8	2.774(3)	S4	2.734(7)	S4	2.965(3)
S16	3.310(3)	S7	3.194(4)	S1	3.091(17)	S4	2.975(3)	S17	2.875(6)	S18	3.004(3)
S9	3.317(2)	S12	3.205(3)	S12	3.192(8)	S18	2.996(3)	S8	2.928(7)	S17	3.030(2)
S15	3.359(2)	S17	3.207(8)	S14	3.223(11)	S17	3.162(3)	S18	3.093(7)	S8	3.091(2)
S17	3.382(2)	S3	3.366(8)	S7	3.331(8)	S13	3.449(3)	S18	3.750(7)	S13	3.192(3)
S7	3.383(2)	S1	3.428(7)	S4	3.691(15)	S2	3.461(3)			S5	3.289(2)
S8	3.396(2)	S4	3.469(4)	S3	3.753(16)	S2	3.683(3)			S14	3.774(3)
S12	3.536(2)	S8	3.549(8)	S8	3.935(17)	S2	3.843(3)			S11	3.930(3)
Sb1–		Sb2–		As3–		As4–		As5–		As6–	
S17	2.423(2)	S7	2.476(2)	S18	2.265(3)	S1	2.279(3)	S14	2.275(3)	S8	2.290(2)
S9	2.524(2)	S7	2.502(2)	S3	2.281(3)	S9	2.299(2)	S4	2.295(3)	S2	2.368(3)
S1	2.602(2)	S12	2.528(2)	S15	2.299(3)	S12	2.310(2)	S16	2.311(3)	S16	2.446(3)
S15	2.845(2)	S3	2.995(2)	S1	3.247(3)	S7	3.142(3)	S2	3.285(3)	S11	2.973(3)
S3	3.050(2)	S1	3.120(2)	S9	3.411(3)	S12	3.226(3)	S11	3.390(3)	S6	3.407(3)
S12	3.664(2)	S9	3.390(2)								
Sb7–		As7–		As8–		Sb9–		As10–		Ag10–	
S6	2.408(4)	S6	2.332(16)	S11	2.270(3)	S5	2.514(3)	S10	2.310(4)	S16	2.661(3)
S5	2.469(4)	S5	2.345(16)	S13	2.299(3)	S14	2.586(3)	S10	2.434(4)	S6	2.710(3)
S11	2.563(4)	S10	2.635(13)	S2	2.340(3)	S13	2.688(3)	S6	2.520(3)	S10	2.722(3)
S10	2.925(4)	S11	2.857(13)	S10	3.464(4)	S10	2.856(3)	S5	2.934(4)	S5	2.815(3)
S2	3.412(4)	S2	3.416(13)	S11	3.574(4)	S6	2.864(3)	S16	3.184(4)	S13	2.866(4)
										S10	2.949(4)

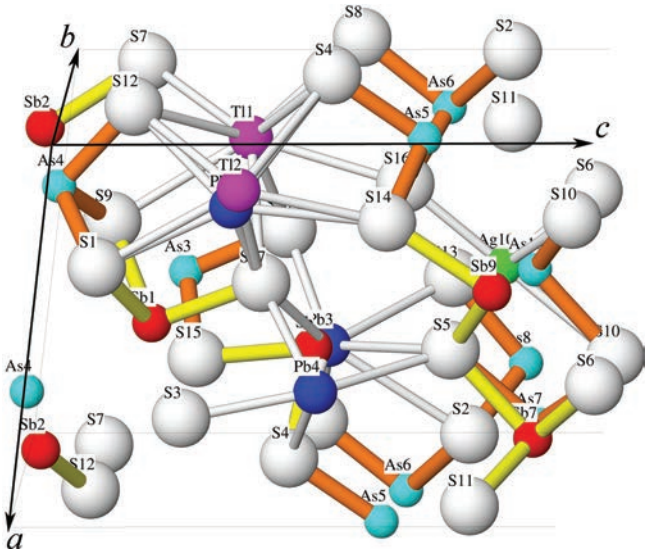

Fig. 6. Atom labelling in the crystal structure of écrinsite. Blue spheres – Pb, magenta spheres – Tl, red spheres – Sb, cyan spheres – As, green spheres – Ag, and white spheres – S. Short As–S bonds are highlighted in rusty brown, short Sb–S bonds in yellow.

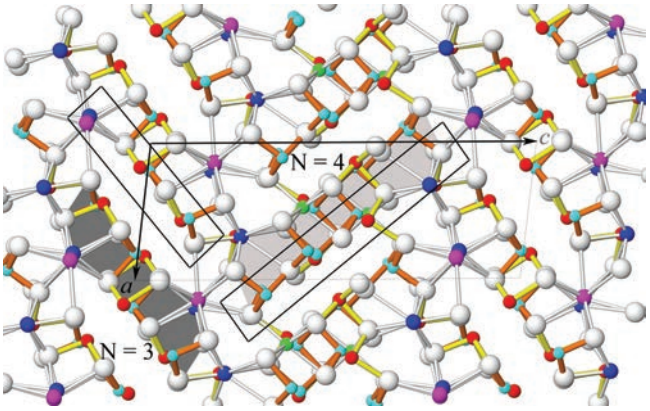

Fig. 7. The crystal structure of écrinsite in projection on (0 1 0) with single chains $N = 3$ and $N = 4$ (SnS-like layers) and ribbons (double-chains) indicated. For conventions see Fig. 6.

A bulk composition of the myrmekitic aggregates was determined by phase analysis of several fragments, using the difference in averaged Z values in back-scattered electron images (as shown in Fig. 4). Measurements were performed with the ICS32 software program from Boerder Electronics (J. Boerder, pers. comm.), on nine selected fragments presented in Fig. 5, without accompanying jasrouxite. Averaged area percentage is: for smithite (blue in Figs. 4 and 5) 21.9% (range 0.75–35.12%), for stibnite (green in Figs. 4 and 5) 38.1% (range 28.5–60.3%), and for écrinsite (red in Figs. 4 and 5) 39.9% (range 24.1–57.5%). These percentages multiplied by element contents in the three phases yield a composition estimate (in wt%) of Ag 16.9, Tl 3.5, Pb 10.7, Sb 26.3, As 16.9, and S 25.8 for the myrmekite bulk, not far from the chemistry of type jasrouxite, Ag 17.5, 0.6 Cu, Tl 0.1, Pb 9.4, Sb 33.6, As 12.8 and S 25.8 wt% (Topa *et al.*, 2013a), but with a distinct enrichment in Tl and As.

Table 8. Bond-valence analysis for écrinsite.[a]

Site	Me1	Me2a	Me2b	Me3a	Me3b	Me4	Me5	Me6	Me7	Me8	Me9	Me10	Me11a	Me11b	Me12	Me13	Me14a	Me14b
Atom	Tl1	Tl2	Pb2	Pb3	Sb	Pb4	Sb1	Sb2	As3	As4	As5	As6	Sb7	As7	As8	Sb9	As10	Ag10
Occup.		0.820	0.180	0.645	0.355								0.770	0.230			0.529	0.471
S1		0.092	0.224				0.709	0.141	0.072	0.981								
S2				0.084							0.065	0.77	0.066	0.045	0.832			
S3		0.110	0.038			0.493	0.211		0.976									
S4	0.143	0.083	0.045	0.039	0.493	0.318					0.940							
S5				0.046		0.132							1.014	0.819		0.900	0.153	0.151
S6													1.195	0.850		0.349	0.469	0.201
S7	0.104	0.173	0.119					0.995		0.095								
								0.930										
S8	0.100	0.067	0.023	0.533	0.385	0.226						0.95						
S9	0.124	0.168					0.874			0.932								
S10													0.296	0.371	0.040	0.365	0.827	0.195
																	0.591	0.105
S11												0.15	0.786	0.208	1.035			
S12	0.069							0.862		0.902								
S13				0.086		0.172									0.932	0.526		0.132
S14		0.191	0.159			0.036					0.992	0.04				0.739		
S15	0.111			0.567	0.989		0.367		0.927	0.032								
S16	0.126			0.030							0.900	0.63					0.078	0.230
S17	0.104	0.167	0.428	0.186	0.267	0.336	1.145											
S18	0.149	0.182	0.249	0.292	0.188				1.016									
Sum	1.03	0.99	0.25	1.19	0.84	1.71	3.31	2.93	2.99	2.94	2.90	2.54[b]	2.59	0.53	2.84	2.88	1.12	0.48
Theor.	1.00	0.82	0.36	1.28	1.08	2.00	3.00	3.00	3.00	3.00	3.00	3.00	2.31	0.69	3.00	3.00	1.59	0.47

[a] Calculations done with VALENCE (Brown, 1996). The sum values were calculated taking into account the refined occupancies.
[b] Taking into account the Sb content of the Me10 site would bring the sum closer to 3.00.

From the point of view of ore genesis, the formation of a part of écrinsite as a component of a three-phase smithite–écrinsite–stibnite aggregate with myrmekitic texture is very intriguing, but difficult to explain. Texture and composition (Figs. 4 and 5) suggest that most probably the aggregate is a product of reaction of earlier formed jasrouxite with Tl-bearing solutions, or results from transformation of a high-temperature precursor phase into the above-mentioned exsolved components.

6. Crystallography and crystal structure

Single-crystal studies were performed on écrinsite fragments, mechanically extracted after microprobe analysis, from samples J5R1 (écrinsite type material, analyses no. 1 and 4 in Table 2) and JR (myrmekite-containing fragments of the jasrouxite type material, analysis no. 5 in Table 2). The present paper deals with the single-crystal study results for the highest Tl-substituted and best preserved écrinsite grain (sample J5R1, analysis no. 1 in Table 2), whereas the other refinements of compositionally different (medium- and low-Tl, Table 2) écrinsite will be used in a separate paper concerning the crystal chemistry of écrinsite and related minerals. This forthcoming paper will also discuss the new crystal-chemical data on boscardinite reported by Biagioni & Moëlo (2017).

A small fragment with good diffracting quality and irregular shape was mounted on a Nonius KappaCCD single-crystal X-ray diffractometer equipped with a CCD detector and a 300 μm diameter capillary-optics collimator to provide increased resolution. The measured intensity data (Mo-$K\alpha$) were processed with the Nonius program suite DENZO-SMN and corrected for Lorentz, polarization, and background effects, and, by the multi-scan method (Otwinowski *et al.*, 2003), for absorption. The centrosymmetric space group $P\bar{1}$ proposed by the XPREP program was chosen. The structure of écrinsite was solved by direct methods (SHELXS-97; Sheldrick, 2008), which revealed most of the atom positions. In subsequent cycles of the refinement (SHELXL-97; Sheldrick, 2008), remaining atom positions were deduced from difference-Fourier syntheses. Occupancies of several split and mixed sites were assigned based on geometric features, bond-valence calculations and crystal-chemical considerations. For easier comparison with the closely related type boscardinite (Orlandi *et al.*, 2012), the coordinate-set of the latter was used for the final refinement cycles. Final refinement yielded $R_1 = 0.0525$ for 6199 reflections with $F_o > 4\sigma(F_o)$ and 0.1231 for all 11 124 data. Crystal data and a summary of parameters describing data collection and refinement are presented in Table 4, atomic coordinates, occupancy factors and displacement parameters in Table 5, selected interatomic distances (Å) in Table 6, and calculated X-ray powder diffraction data in Table 7 (deposited, not printed, linked to this article and freely available online, http://eurjmin.geoscienceworld.org). A bond-valence analysis is presented in Table 8.

Table 9. Comparative data for écrinsite and related sartorite homologues with $N = 3.5$.

Mineral	Écrinsite	Boscardinite	Bernarlottiite	Argentobaumhauerite	Baumhauerite
Ideal formula	$AgTl_3Pb_4As_{11}Sb_9S_{36}$	$Tl_2Pb_8Sb_{14}As_4S_{36}$	$Pb_{12}As_{10}Sb_6S_{36}$	$AgPb_{22}As_{33}S_{72}$	$Pb_{12}As_{16}S_{36}$
Crystal system	Triclinic	Triclinic	Triclinic	Triclinic	Triclinic
Space group	*P*1	*P*1	*P*1	*P*1	*P*1
Superstructure			Threefold *a*	Twofold *c*	
Unit-cell parameters					
a (Å)	8.080(2)	8.0929(4)	23.704(8)	7.905(1)	7.884(4)
b (Å)	8.533(2)	8.7610(5)	8.386(2)	8.468(1)	8.345(4)
c (Å)	22.613(4)	22.4971(11)	23.501(8)	44.410(5)	22.811(11)
α (°)	90.23(3)	90.868(4)	89.91(1)	84.614(2)	90.069(8)
β (°)	97.17(3)	97.247(4)	102.93(1)	86.496(2)	97.255(8)
γ (°)	90.83(3)	90.793(4)	89.88(1)	89.810(2)	90.082(8)
V (Å^3)	1546.7(6)	1582.0(2)	–	2954.2(6)	1488.8(13)
R_1	5.25	4.5	–	3.49	5.00
Z	1	1	3	1	1
Reference[a]	1	2	3	4	4

[a] 1 – this study; 2 – Orlandi *et al.* (2012); 3 – Orlandi *et al.* (2017); 4 – Topa & Makovicky (2016).

The structure of écrinsite contains 14 independent metal and 18 distinct sulphur sites (Table 5 and Fig. 6). There are five fully occupied sites (Tl1, Pb4, Sb1, Sb2 and As4) and nine mixed sites of which four are split: (Tl,Pb)2, (Pb3, Sb), (Sb,As)7 and (As,Ag)10. The final scheme of site occupancies for mixed sites and splitting of certain sites is an output of a combination between obtained bond-lengths and measured chemistry. The slightly unbalanced charge (+0.89) in the structural formula, $Ag_{0.94}Tl_{3.63}Pb_{3.66}(Sb_{9.43}As_{10.33})_{\sum 19.76}S_{36}$ is due to over-estimation of the refined Tl2 content in the split site (Tl,Pb)2. In spite of complicated site occupancies, écrinsite shows bond-valence values close to expected numbers (Table 8).

The zig-zag walls composed of tricapped trigonal coordination prisms, which characterize the majority of sartorite homologues, are modified in écrinsite by Tl- and Sb-substitutions, respectively (Fig. 7). Columns with a combination of Tl1 and (Tl,Pb)2 prisms alternate with those containing (Pb,Sb)3 and Pb4 prisms. The mixed sites were defined as split positions, with the positions of the dominant cations coming out better determined than the non-dominant ones; the Sb3 site could even be slightly split and disordered between two alternative close positions. The Tl- and (Tl,Pb)-centred polyhedra exhibit appropriate changes in Me–S distances, in agreement with their occupancies (Tables 5 and 6).

The configurations in the $N = 3$ slab of the écrinsite structure (Fig. 8) tend towards a bond topology similar to that of the $N = 3$ slab in guettardite and twinnite (Makovicky & Topa, 2012; Makovicky *et al.*, 2012). In the surface of a tightly bonded double ribbon, the marginal, side-bonded As3 site ($As_{0.82}Sb_{0.18}$) is separated in écrinsite by a distance of 4.25 Å from a Sb1 site (100% Sb), which shows signs of possible positional disorder along the line S1 (bond length 2.60 Å)–S15 (bond length 2.85 Å). The S15 atom associates with the side-bonded As4 site via short bonds to S1 and S9. The Sb1–As4 distance is 3.45 Å and the Sb1–As4 group is almost symmetrical. The 2.85 Å Sb1–S15 distance can be compared with the 3.05 Å distance to S3 in the other As3-centred polyhedron, corroborating the suggested weak amount of flipping of the Sb1 atom to the alternative, S15-oriented, bond scheme. This situation scheme results in a (poorly defined) diagonally orientated three-cation crankshaft chain. This configuration is faced in the same ribbon surface by a single Sb2 site associated with the $(Pb_{0.19}Tl_{0.81})2$ site. The alternating, large Tl1 site faces long As–S distances of the As4-centred polyhedron.

In the closely similar structure of type boscardinite (Orlandi *et al.*, 2012), the $N = 3$ chain is composed of the Sb3 ($Sb_{0.71}As_{0.29}$)–Sb1–As4 ($As_{0.75}Sb_{0.25}$)-centred polyhedra, the opposing polyhedron is Sb2-centred and the large $(Tl_{0.8}Pb_{0.2})1$-centred polyhedron is placed in the same position as the Tl1-centred one in écrinsite (Fig. 8). However, here the flipping of the Sb1 site is more pronounced, the connection to the Sb3-centred polyhedron is 2.77 Å (countered by 2.67 Å in the Sb1–As4 pair). In guettardite (Makovicky *et al.*, 2012), the corresponding chain is As2 (sof 1.05)–typical flipping Sb2 (sof 0.94)–As1 (sof 0.98), whereas the lone polyhedron is centred by Sb1 (sof 0.98; the refined sof values express the weak Sb–As mixing in the sites). The size difference between the Pb1- and Pb2-centred polyhedra in guettardite is small; they both adjust by distorting their ideal prismatic shape. In the related twinnite (Makovicky & Topa, 2012) the chain starts with $(As_{0.62}Sb_{0.38})6$, continues via flipping bonds of the Sb4 site to the $(As_{0.87}Sb_{0.13})5$ site; the opposing sole polyhedron is centred by Sb3. The shortest bonds of these Sb4, As5 and Sb3 sites correlate in their lengths in order to produce a narrow crankshaft chain.

In the $N = 4$ slab of écrinsite (Fig. 9) a diagonal chain is developed, starting with side-bonded As5 ($As_{0.85}Sb_{0.15}$), followed by a mixed As6 site ($As_{0.67}Sb_{0.33}$) with a partly flipping character. This is suggested by the As6–S11 2.97 Å bond, opposed by a 2.45 Å bond to S16, whereas the unaffected 2.37 Å As6–S2 distance is opposed by the

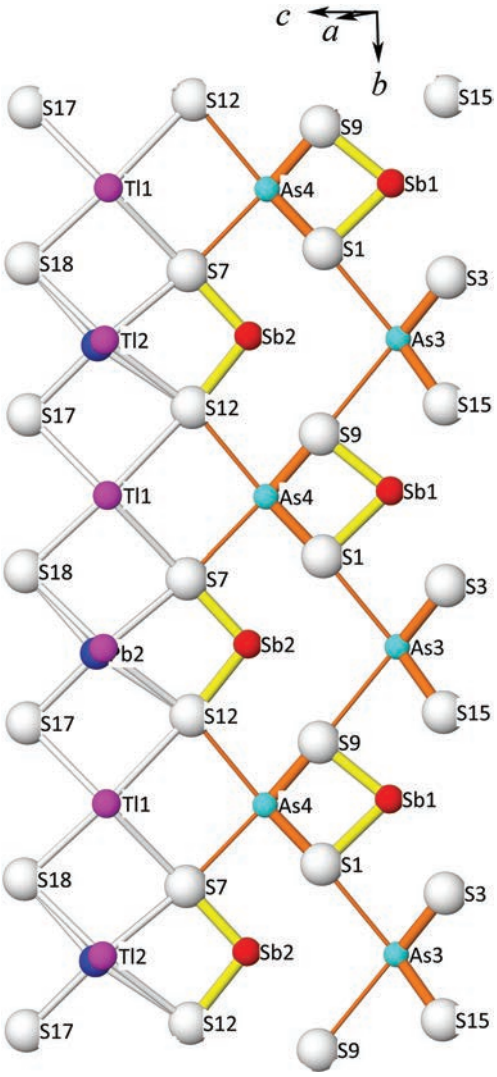

Fig. 8. A single-atom deep surface of the ribbon with $N=3$. For conventions see Fig. 6.

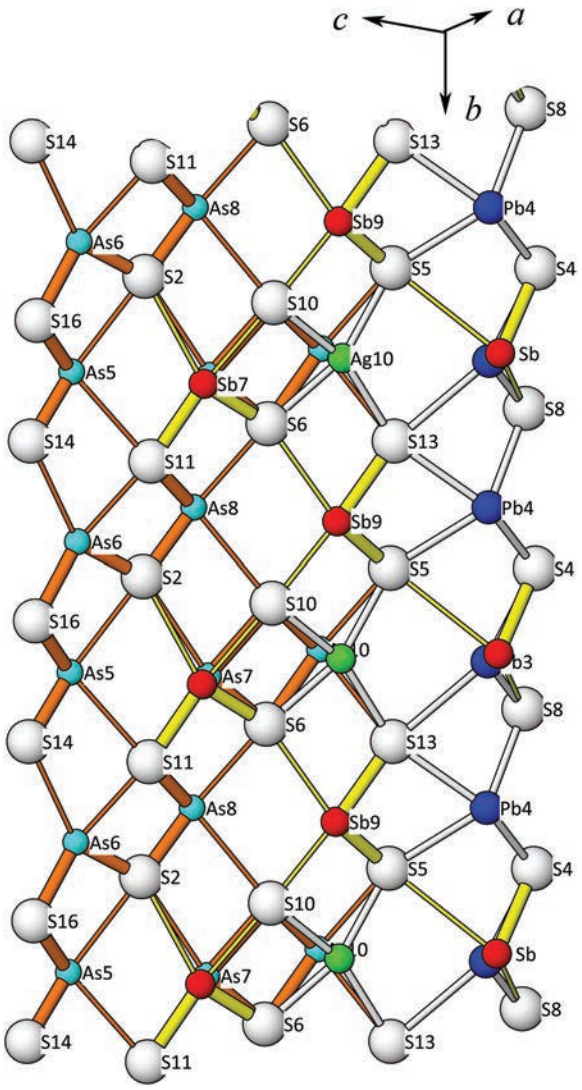

Fig. 9. A single-atom deep surface of the ribbon with $N=4$. Double-cation sites are mixed sites in the same coordination polyhedron. For conventions see Fig. 6.

3.43 Å distance to S14. The As8 site is well defined and strongly As-dominant ($As_{0.86}Sb_{0.14}$), and the following fractionally occupied Sb7 site ($Sb_{0.77}$) is "bottom"-bonded via 2.41 and 2.56 Å bonds (the remaining As7 portion, $As_{0.23}$, of this split site was refined as side-bonded, with bonds of 2.33 and 2.64 Å). The Me7-centred polyhedron is followed by a split Me10 site ($As10_{0.53}/Ag10_{0.47}$). The next Sb site, Sb9 ($Sb_{0.81}As_{0.19}$), has an indistinctly flipping character. Together, these cations form a five-membered chain, with an As7–As10 pair tied together via short As–S bonds. The latter is facing the mixed, split (Pb3,Sb) site ($Pb3_{0.64}$ and $Sb_{0.36}$). The next Sb site, Sb9 ($Sb_{0.81}As_{0.19}$) is separated from the chain by long Sb–S distances and has an indistinctly flipping character.

In type boscardinite, the corresponding chain is composed of the sequence Sb5 ($Sb_{0.78}As_{0.22}$)–Sb6–Sb8 ($Sb_{0.53}As_{0.47}$)–Sb7 (with a bond-scheme flipping character) – 0.71 Sb10 & 0.29 Ag10–0.81 Sb9 & 0.19 Pb9. The latter two sites are mixed sites with separately positioned and refined cations. The split Sb9/Pb9 site faces the Pb3 site from the column of Pb trigonal prisms.

The silver substitution appears at the same site in écrinsite (Ag10 in Fig. 8) and type boscardinite. Principal differences between the chains in the two structures are connected with different bonding schemes of As and Sb, respectively, and only vaguely parallel variations in the As/Sb ratios of individual cation sites in the above chains.

Crankshaft chains in tightly bonded double-ribbons with $N=3$ and 4, respectively, are illustrated in Fig. 10, which shows a fragment of the écrinsite structure with both $N=3$ and $N=4$ slabs projected on (1 0 0). Although subparallel in Fig. 10, the two chains belong to adjacent double-ribbons that are perpendicular to one another, as seen in Fig. 7.

Table 10. Comparison of site occupancies (except 18 S sites) for type boscardinite and écrinsite.

Ref.	Boscardinite Orlandi *et al.* (2012)		Écrinsite This work
Site label		Site label	
(**Tl**,Pb)1	$Tl_{0.8}Pb_{0.2}$	**Tl**1	$Tl_{1.00}$
(**Pb**,Tl)2a	$Pb_{0.27}Tl_{0.11}$	**Tl**2	$Tl_{0.82}$
(**Pb**,Tl)2b	$Pb_{0.50}Tl_{0.12}$	**Pb**2	$Pb_{0.18}$
(**Pb**,Tl)3	$Pb_{0.80}Tl_{0.20}$	(**Pb**,Sb)3	$Pb_{0.635}Sb_{0.355}$ (split)
Pb4	$Pb_{1.00}$	**Pb**4	$Pb_{1.00}$
Sb1	$Sb_{1.00}$	**Sb**1	$Sb_{1.00}$
Sb2	$Sb_{1.00}$	**Sb**2	$Sb_{1.00}$
(**Sb**,As)3	$Sb_{0.71(1)}As_{0.29(1)}$	(**As**,Sb)3	$As_{0.80}Sb_{0.20}$
(**As**,Sb)4	$As_{0.75(1)}Sb_{0.25(1)}$	**As**4	$As_{1.00}$
(**Sb**,As)5	$Sb_{0.78(1)}As_{0.22(1)}$	(**As**,Sb)5	$As_{0.85}Sb_{0.15}$
Sb6	$Sb_{1.00}$	(**As**,Sb)6	$As_{0.66}Sb_{0.34}$
Sb7	$Sb_{1.00}$	(**Sb**,As)7	$Sb_{0.77}As_{0.23}$ (split)
(**Sb**,As)8	$Sb_{0.53(1)}As_{0.47(1)}$	(**As**,Sb)8	$As_{0.89}Sb_{0.11}$
Sb9	$Sb_{0.814(5)}Pb_{0.186(5)}$ (split)	(**Sb**,As)9	$Sb_{0.80}As_{0.20}$
Sb10	$Sb_{0.71(3)}Ag_{0.29(3)}$ (split)	(**As**,Ag)10	$As_{0.53}Ag_{0.47}$ (split)

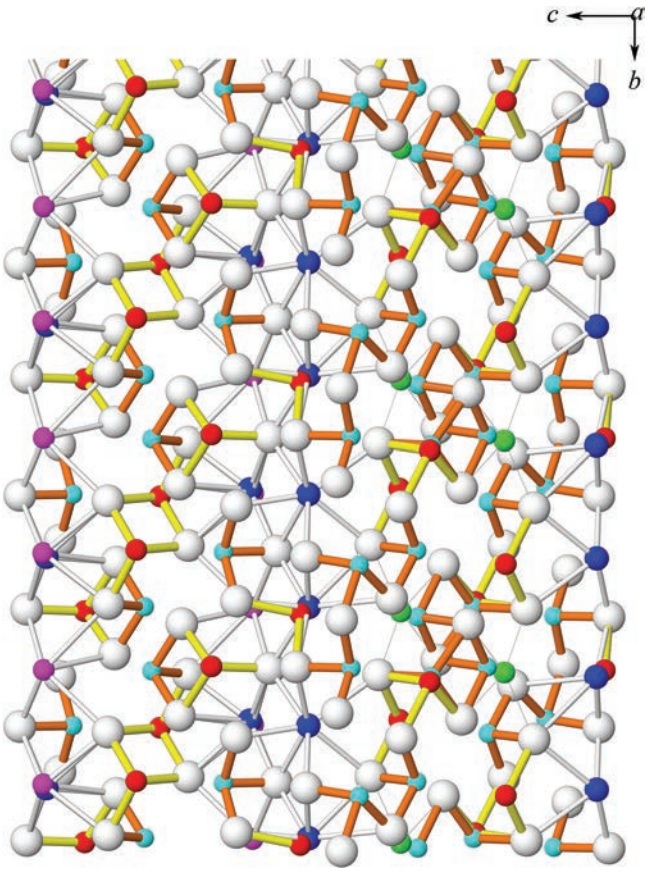

Fig. 10. A (1 0 0) slice of the écrinsite structure displaying a double layer with $N = 3$ along the left-hand side and that with $N = 4$ along the right-hand side of the figure, with As–S and Sb–S bonds defining complex crank-shaft chains, running diagonally in a full double-layer thickness. For conventions see Fig. 6.

7. Position within the sartorite homologous series (with $N = 3.5$)

As mentioned above, écrinsite compares with several $N_{1,2} = 3$, 4 (*i.e.*, $N = 3.5$) sartorite homologues (baumhauerite, argentobaumhauerite, boscardinite and bernarlottiite – Table 9 and Fig. 3). There are however clear distinctions among them.

Two of them display superstructures: argentobaumhauerite, which accommodates small amounts of Ag, has a doubled *c* parameter (44.4 Å instead of 22.8 Å in baumhauerite), and bernarlottiite in which the distribution of Sb and As causes a tripled *a* parameter (23.5 Å instead of ~7.9 Å). Such phenomena have not been found in the structure of écrinsite.

By comparison to the closely related boscardinite, the truly distinctive feature of écrinsite is the dominance of As over Sb: écrinsite is an As-dominant phase (As > Sb) for all six analyzed grain groups, whereas boscardinite is Sb-dominant (Sb ≫ As). The Sb/As ratio of écrinsite (9/11) is substantially different from that in boscardinite, which ranges between 14/4 (sample 4977 – Orlandi *et al.*, 2012) and 14/6 (in Tl- and As-rich varieties – Biagioni & Moëlo, 2017). This difference is reflected in the occupancy of several semimetal sites, which are occupied either fully or predominantly by As in écrinsite, whereas the same sites are all Sb-dominant in type boscardinite (Table 10). Besides, écrinsite has a substitution range of $(Tl,Ag)^{+} + As^{3+}$ for $2Pb^{2+}$ distinctly higher (>50%) than the type boscardinite (<50%, Orlandi *et al.,* 2012) (Figs. 2 and 3) but which is actually matched by the (Tl,As)-rich boscardinite varieties described by Biagioni & Moëlo (2017). Baumhauerite and bernarlottiite are unsubstituted (or both can be very modestly Ag–Tl-substituted). Argentobaumhauerite shows no Tl substitution (Topa & Makovicky, 2016).

8. Dedication

This paper is dedicated to the memory of our treasured friend and colleague, Dr. Zdeněk Johan, a Czech and French mineralogist with a special attachment to the study of minerals from the Jas Roux locality.

Acknowledgements: The authors express their gratitude to all the above listed donors who contributed material to this study. We thank Clemens Schalko for his technical assistance. We also thank the administration of the Parc national des Écrins for the permit to conduct a mineralogical study of the Jas Roux deposit. Jean-Claude Boulliard helped to obtain this permit and G. Favreau and V. Bourgoin helped with field work. The paper was handled by Reto Gieré and the comments of Nicolas Meisser and an anonymous reviewer helped to improve the paper.

References

Biagioni, C. & Moëlo, Y. (2017): Lead-antimony sulfosalts from Tuscany (Italy). XVIII. New data on the crystal-chemistry of boscardinite. *Mineral. Mag*., **81**, 47–60.

Biagioni, C., Orlandi, P., Moëlo, Y., Bindi, L. (2014): Lead-antimony sulfosalts from Tuscany (Italy). XVI. Carducciite, $(AgSb)Pb_6(As,Sb)_8S_{20}$, a new Sb-rich derivative of rathite from the Pollone mine, Valdicastello Carducci: occurrence and crystal structure. *Mineral. Mag.*, **78**, 1775–1793.

Bourgoin, V., Favreau, G., Boulliard, J.-C. (2011): Jas Roux (Hautes-Alpes): un gisement exceptionnel à minéraux de thallium. *Le Cahier des Micromonteurs*, no. **113**, 2–92.

Brown, I.D. (1996): VALENCE: a program for calculating bond valences. *J. Appl. Crystallogr.*, **29**, 479–480.

Graeser, S., Paar, W.H., Chen, T.T. (1986): Baumhauerit: ein zweites Vorkommen (Salzburg, Austria). *Schweiz. Mineral. Petrogr. Mitt.*, **66**, 259–266.

Johan, Z. & Mantienne, J. (2000): Thallium-rich mineralization at Jas Roux, Hautes-Alpes, France: a complex epithermal, sediment-hosted, ore-forming system. *J. Czech Geol. Soc.*, **45**, 63–77.

Kraus, W. & Nolze, G. (1999): PowderCell 2.3. Federal Institute for Materials Research and Testing, Berlin, Germany.

Makovicky, E. (1985): The building principles and classification of sulphosalts based on the SnS archetype. *Fortschr. Mineral.*, **63**, 45–89.

Makovicky, E. & Topa, D. (2012): Twinnite, $Pb_{0.8}Tl_{0.1}Sb_{1.3}As_{0.80}S_4$, the OD character and the question of its polytypism. *Z. Kristallogr.*, **227**, 468–475.

—, — (2015): Crystal chemical formula for sartorite homologues. *Mineral. Mag.*, **79**, 25–31.

Makovicky, E., Topa, D., Tajjedin, H., Rastad, E., Yaghubpur, A. (2012): The crystal structure of guettardite, $PbAsSbS_4$. *Can. Mineral.*, **50**, 253–265.

Mantienne, J. (1974): La minéralisation thallifère de Jas Roux (Hautes Alpes). Doctorate thesis, Université de Paris VI, 153 p. https://tel.archives-ouvertes.fr/tel-00795085/.

Moëlo, Y., Makovicky, E., Mozgova, N.N., Jambor, J.L., Cook, N., Pring, A., Paar, W., Nickel, E.H., Graeser, S., Karup-Møller, S., Balić-Žunić, T., Mumme, W.G., Vurro, F., Topa, D., Bindi, L., Bente, K., Shimizu, M. (2008): Sulfosalt systematics: a review. Report of the sulfosalt sub-committee of the IMA commission on ore mineralogy. *Eur. J. Mineral.*, **20**, 7–46.

Orlandi, P., Biagioni, C., Bonaccorsi, E., Moëlo, Y., Paar, W.H. (2012): Lead–antimony sulfosalts from Tuscany (Italy). XII. Boscardinite, $TlPb_3(Sb_7As_2)_{\Sigma 9}S_{18}$, a new mineral species from the Monte Arsiccio mine: occurrence and crystal structure. *Can. Mineral.*, **50**, 235–251.

—, —, —, —, — (2017): Lead–antimony sulphosalts from Tuscany (Italy). XXI. Bernarlottiite, $Pb_{12}(As_{10}Sb_6)_{\Sigma 16}S_{36}$, a new $N = 3.5$ member of the sartorite homologous series from the Ceragiola marble quarry: occurrence and crystal structure. *Eur. J. Mineral.*, **29** (this issue). DOI:10.1127/ejm/2017/0029-2625.

Otwinowski, Z., Borek, D., Majewski, W., Minor, W. (2003): Multiparametric scaling of diffraction intensities. *Acta Crystallogr.*, **A59**, 228–234.

Saliot, P., Guilhaumou, N., Barbillat, J. (1982): Les inclusions fluides dans les minéraux du métamorphisme à laumontite-prehnite-pumpellyite des grès du Champsaur (Alpes du Dauphiné). Etude du mécanisme de circulation des fluides. *Bull. Minéral*., **105**, 648–657.

Sheldrick, G.M. (2008): A short history of *SHELX*. *Acta Crystallogr.*, **A64**, 112–122.

Stalder, P.J. (1979): Organic and inorganic metamorphism in the Taveyannaz sandstone of the Swiss Alps and equivalent sansdstones in France and Italy. *J. Sedim. Petrol.*, **49**, 463–482.

Topa, D. & Makovicky, E. (2016): Argentobaumhauerite: name, chemistry, crystal structure, comparison with baumhauerite, and position in the Lengenbach mineralization sequence. *Mineral. Mag.*, **80**, 819–840.

Topa, D., Makovicky, E., Favreau, G., Bourgoin, V., Boulliard, J.-C. (2013a): Jasrouxite, a new Pb-Ag-As-Sb member of the lillianite homologous series from Jas Roux, Hautes-Alpes, France. *Eur. J. Mineral.*, **25**, 1031–1038.

Topa, D., Makovicky, E., Tajedin, H., Putz, H., Zagler, G. (2013b): Barikaite, $Ag_3Pb_{10}(Sb_8As_{11})_{\Sigma 19}S_{40}$, a new member of the sartorite homologous series. *Mineral. Mag.*, **77**, 3039–3046.

Topa, D., Keutsch, F.N., Makovicky, E., Kolitsch, U., Paar, H.W. (2017): Polloneite, a new complex Pb(–Ag)–As–Sb sulfosalt from the Pollone mine, Apuan Alps, Tuscany, Italy. *Mineral. Mag.*, **81**, DOI:10.1180/minmag.2017.081.003.

Received 9 December 2016
Modified version received 2 March 2017
Accepted 4 March 2017